Numerical Simulation of Evaporating Sprays in a Convective Flow Field

R. M. Humza*, S. R. Gopireddy, E. Gutheil
Interdisciplinary Center for Scientific Computing, University of Heidelberg, Germany
rana.humza@iwr.uni-heidelberg.de, srikanth.reddyg@iwr.uni-heidelberg.de and
gutheil@iwr.uni-heidelberg.de

Abstract

In the present work, the direct quadrature method of moments (DQMOM) and the discrete droplet model (DDM) in an axisymmetric, two-dimensional configuration are used to model an evaporating water spray carried by nitrogen, the spray is injected into a vertical spray chamber. The models include the Abramzon and Sirignano model for convective droplet evaporation, while droplet motion is included by considering droplet drag and gravity. In DDM, the effects of the two-phase flow are captured by resolving the gas phase conservation equations considering the droplets as point sources. DQMOM considers the inlet gas flow properties to compute the drag force exerted on the droplet velocity. The phenomena of droplet – droplet interactions are currently neglected as the liquid volume in the present case is small. Appropriate initial and boundary conditions as well as the starting values for simulations are generated from experimental data, which have been carried out at TU Graz, Austria by the group of Prof. G. Brenn. The experimental measurements were performed with phase Doppler anemometry (PDA). The experiment gives the spray characteristics (droplet size and velocity) at different cross sections away from nozzle exit. The DQMOM and DDM simulation results are compared with experimental data at these cross sections, and very good agreement with experiment is observed.

Introduction

The droplet size distribution and interaction of the liquid phase and the gas flow are key features in the modeling of evaporating spray flows, which are important because of their vast range of industrial and engineering applications. Two-phase effects and poly-dispersity of droplet size distributions dominate the structure of any spray and related applications such as spray flames, end products or spray drying processes, or medical applications. The spray dynamics depends on various physical processes such as droplet inertia, evaporation, and gas phase characteristics. Thus, it is important to have reliable models and numerical techniques in order to be able to describe the physics of two-phase flows, where the dispersed phase consists of droplets of various sizes that may evaporate, coalesce, breakup as well as have their own inertia and size-conditioned dynamics.

In recent years, the Euler–Euler approaches have been extensively discussed to model the spray flows because of their numerical ease and computational efficiency. For instance, in the multi-fluid approach [1], the droplet size distribution function is discretized using a finite volume technique that yields conservation equations for mass and momentum of droplets in fixed size intervals called sections or fluids [4]. This approach has recently been extended to higher order of accuracy [5], but discretization of droplet size phase-space is still a problem that needs to be addressed. The efficiency and applicability of moment based methods [2, 3] for multivariate poly-disperse systems have remained a question of interest [6]. In order to address these issues, DQMOM has turned out to be an attractive and suitable approach [7]. However, the advantages of Eulerian–Lagrangian formulations cannot be neglected [8, 9, 10]. The study of a spray flow at a single droplet level is much more informative than most of the formulations used in Eulerian approaches.

The present work focuses on description of spray properties by means of DQMOM [11] and DDM [12], where droplet motion evolves due to interactive drag with ambient gas and gravity. Evaporation is included by applying two film convective droplet evaporation model [13], which considers effects of convection around the evaporating droplets and Stefan flow, and it accounts for variable properties of both the liquid and in the film surrounding the droplet. The initial data for computations are generated using the experimental data, which were measured by the group of Prof. G. Brenn at TU Graz, Austria. The numerical results from both approaches are compared with experimental data at various cross sections downstream the nozzle exit.

The reference experimental setup of the present work is explained in the next section, which is followed by the section describing the mathematical models. In the later sections, the results are presented, discussed and finally concluded.

*Corresponding author: rana.humza@iwr.uni-heidelberg.de

Experimental Setup

A series of experiments had been carried out at TU Graz by the group of Prof. G. Brenn. A water spray in nitrogen was studied for different liquid mass inflow rates. Various atomizers with different dimensions of swirl chambers and exit diameters were used. The droplet sizes and velocities were recorded at various cross sections for different liquid inflow rates using phase Doppler anemometry (PDA) [14]. The present simulations concern the experimental data generated using the Delavan nozzle SDX-SD-90 with an internal diameter of 0.002 m and an outer diameter of 0.012 m at the nozzle throat and 0.016 m at the top for a liquid inflow rate of 80 kg/h. A water spray was injected into a cylindrical spray chamber of diameter 1 m. The carrier gas was nitrogen at room temperature and atmospheric pressure. Measurements were recorded at cross sections of 0.08 m, 0.12 m and 0.16 m. The data at 0.08 m were taken as starting point for initial data generation for computations, and results were compared at later cross sections.

Mathematical Model

In the present work, DQMOM and DDM are applied to model the dilute spray flow in an axisymmetric two-dimensional geometrical configuration. Thus, droplet – droplet interactions are neglected in both approaches. DQMOM accounts for droplet number density, droplet size and velocity, where evaporation and droplet motion are taken into account, the latter one is achieved through inclusion of drag force and gravity. Moreover, the gas phase equations are not solved for DQMOM in the present work rather the inlet gas flow properties are taken for computing the droplet velocity in terms of drag force per unit mass. DDM considers the effects of the two-phase flow by evaluating the source terms for the gas phase conservation equations using particle-source-in-cell (PSIC) model [15]. The mathematical formulation of the models is given in the following subsections.

Direct Quadrature Method of Moments – DQMOM

The DQMOM transport equations are derived from Williams' spray equation [16], which is given by

$$\frac{\partial f}{\partial t} + \frac{\partial (\mathbf{v} f)}{\partial \mathbf{x}} = -\frac{\partial \left(R f\right)}{\partial r} - \frac{\partial (\mathbf{F} f)}{\partial \mathbf{v}} + Q_f + \Gamma_f. \tag{1}$$

The equation describes the transport of the number density function $f(r, \mathbf{v}; \mathbf{x}, t)$ in terms of time, t, and Euclidean space, $\mathbf{x}$. In equation (1), $\mathbf{v}$ and $\mathbf{F}$ denote droplet velocity and drag force per unit mass whereas R is the change of the droplet radius with time, i.e. $R = dr/dt$, where r is the droplet radius. The last two terms refer to the droplet interactions. Q_f represents the increase in f with time due to droplet formation or destruction by processes such as nucleation or breakup whereas Γ_f denotes the rate of change of f caused by collisions with other droplets.

For the present study, a joint radius-velocity number density function is considered, which is approximated by DQMOM as sum of the product of weighted Dirac-delta functions [18] of radii and velocities [7]

$$f(r, \mathbf{v}) = \sum_{n=1}^{N} w_n \delta(r - r_n) \delta(\mathbf{v} - \mathbf{v}_n), \tag{2}$$

where w_n and r_n are chosen as N representative quantities of weights and radii, and $\mathbf{v}_n$ are the corresponding velocities. Application of DQMOM results in closed transport equations for droplet weights or number density, radii and velocities, respectively, which are written as

$$\frac{\partial w_n}{\partial t} + \frac{\partial (w_n \mathbf{v}_n)}{\partial \mathbf{x}} = a_n, \tag{3}$$

$$\frac{\partial (w_n \rho_l r_n)}{\partial t} + \frac{\partial (w_n \rho_l r_n \mathbf{v}_n)}{\partial \mathbf{x}} = \rho_l b_n, \tag{4}$$

and

$$\frac{\partial (w_n \rho_l r_n \mathbf{v}_n)}{\partial t} + \frac{\partial (w_n \rho_l r_n \mathbf{v}_n \mathbf{v}_n)}{\partial \mathbf{x}} = \rho_l \mathbf{c}_n, \tag{5}$$

where a_n, b_n and $\mathbf{c}_n$ are the source terms that may account for evaporation, drag force and gravity.

The steady form of Eqs. (3) – (5) is solved simultaneously by using appropriate initial and boundary conditions to find $w_n(\mathbf{x}, t)$, $r_n(\mathbf{x}, t)$ and $\mathbf{v}_n(\mathbf{x}, t)$, which assume that the droplet radii, velocities and their corresponding

number densities at the inlet plane are set to their initial values generated from experimental data, whereas a free boundary is assumed for the wall and exit plane. If droplets hit the axis of symmetry, they are reflected. An equidistant rectangular grid is adapted, where the size of each grid cell is 1.5 10^{-3} m in radial direction and 1.0 10^{-4} m in axial direction, resulting in a maximum grid of about 80×1000 grid nodes. Equations (3) – (5) are closed by modeling the source terms i.e. a_n, b_n and $\mathbf{c}_n$, using the physical models to account for effects of droplet evaporation, drag force and gravity. These source terms are calculated through moment transformation of phase-space terms, which yields the following linear system

$$P_{k,l} = \int r^k \mathbf{v}^l \left[-\frac{\partial (Rf)}{\partial r} - \frac{\partial (\mathbf{F} f)}{\partial \mathbf{v}} \right] \mathrm{d}r\mathrm{d}\mathbf{v}. \tag{6}$$

The exact form of the DQMOM linear system relies on the choice of moments. To obtain a solution, the moments are so chosen that the resulting coefficient matrix is non-singular. In the present work, N is set to be 3 and the corresponding moment set is chosen as [18] $k \in \{1, ..., 2N\}$; $l \in \{0, 1\}$. Though this approach has been tested to model non-evaporating sprays [19, 20, 21], few studies have been carried out on evaporating sprays [18, 22, 23]. However, these studies consider a very simplified evaporation model to calculate the change in droplet size with time i.e. either as a linear function of droplet volume or non-linear function of droplet volume, which is similar to the well established but very simplified d^2 law. This has been improved [11] by implementing the advanced evaporation model. Droplet evaporation is accounted for by considering the rate of change of droplet volume as [13]

$$\dot{m} = -\frac{\mathrm{d}}{\mathrm{d}t} \left(\frac{4}{3} \pi r^3 \rho_l \right) = 2\pi r (\bar{\rho} \bar{D})_f \widetilde{\mathrm{Sh}} \, \ln(1 + B_M). \tag{7}$$

Here, subscript f refers to properties in the film, $\widetilde{\mathrm{Sh}}$ is the modified Sherwood number and B_M is the Spalding mass transfer number, which is calculated as

$$B_M = \frac{Y_s - Y_\infty}{1 - Y_s}, \tag{8}$$

where Y_s and Y_∞ are mass fractions of the vapor at the droplet surface and in the bulk of surrounding gas, respectively, and, following Dalton's law [24], Y_s is given by

$$Y_s = \frac{M_L}{M_L + M(p/p_L - 1)}. \tag{9}$$

The quantities M_L and p_L denote molar mass and vapor pressure of water, while M and p represent molar mass of the surrounding gas and atmospheric pressure, respectively. Vapor pressure of water is calculated using Antoine's equation [25]. The evaporative flux is computed using the ratio constraints of weights, radii and velocities as introduced by Fox et al. [18].

Assuming the droplet velocity to evolve by interactive drag applied by the surrounding gas and gravity, the following relation is used to express the equation of droplet motion [26]

$$\frac{\mathrm{d}\mathbf{v}}{\mathrm{d}t} = \frac{3}{8} \frac{1}{r} \frac{\rho_g}{\rho_l} (\mathbf{u} - \mathbf{v}) |\mathbf{u} - \mathbf{v}| C_D + g, \tag{10}$$

where ρ_g and $\mathbf{u}$ are the density and velocity of the surrounding gas, while ρ_l, C_D, and g are liquid density, drag coefficient, and gravitational acceleration, respectively. The drag coefficient C_D is calculated as a function of the droplet Reynolds number, $\mathrm{Re}_d = 2r\rho_g |\mathbf{u} - \mathbf{v}| / \mu_f$, where μ_f is the mean dynamic viscosity in the film, as [27]

$$C_D = \begin{cases} \frac{24}{\mathrm{Re}_d} \left(1 + 0.15 \, \mathrm{Re}_d^{0.687} \right) & \text{if } \mathrm{Re}_d < 10^3 \\ 0.44 & \text{if } \mathrm{Re}_d \geq 10^3 \end{cases}. \tag{11}$$

Discrete Droplet Model – DDM

For generality, the mathematical formulation for the gas phase uses Favre-averaged variables even though the present application does not include strong effects of compressibility. The steady Favre-averaged Navier-Stokes equations in an axisymmetric, two-dimensional configuration with no swirl for a dilute spray yield

$$\frac{\partial(\bar{\rho}_g \widetilde{u}_x \tilde{\Phi})}{\partial x} + \frac{1}{r}\frac{\partial(r\bar{\rho}_g \tilde{u}_r \tilde{\Phi})}{\partial r} - \frac{\partial}{\partial x}\left(\Gamma_{\Phi,\mathrm{eff}}\frac{\partial \tilde{\Phi}}{\partial x}\right) - \frac{1}{r}\frac{\partial}{\partial r}\left(r\Gamma_{\Phi,\mathrm{eff}}\frac{\partial \tilde{\Phi}}{\partial r}\right) = \bar{S}_{g,\tilde{\Phi}} + \bar{S}_{l,\tilde{\Phi}}, \tag{12}$$

which are closed with an extended $k-\epsilon$ model [17]. In Eq. (12), ρ_g, u_x, and u_r are the gas density, and axial and radial components of the gas velocity, respectively. k and ϵ are the turbulent kinetic energy and the turbulent dissipation rate. $\Gamma_{\Phi,\mathrm{eff}}$ denotes the effective exchange coefficient of variable Φ. $S_{g,\tilde{\Phi}}$ and $S_{l,\tilde{\Phi}}$ are the source terms of gas and liquid phases, which are formulated as described by Hollmann and Gutheil [17]. The replacement of Φ with $1, u_x, u_r, h, k$, and ϵ yields the conservation equations of mass, momentum, energy, turbulent kinetic energy, and the turbulent dissipation rate, respectively. The effective exchange coefficient $\Gamma_{\Phi,\mathrm{eff}}$ is given by

$$\Gamma_{\Phi,\mathrm{eff}} = \frac{\mu_l}{\sigma_{\Phi,l}} + \frac{\mu_t}{\sigma_{\Phi,t}}, \tag{13}$$

where μ_l and μ_t are the molecular and turbulent dynamic viscosities of the gas with $\mu_t = C_\mu \bar{\rho}_g \tilde{k}^2/\tilde{\epsilon}$, and σ_Φ are the corresponding Prandtl-Schmidt numbers. For more details, see Hollmann and Gutheil [17].

The DDM uses the Lagrangian particle tracking method. Literature on DDM [12, 28, 29] proves its suitability for dilute sprays where droplet – droplet interactions may be neglected. The droplet sizes and velocities are solved by use of Eqs. (7) – (11). The numerical time step for the governing equations is controlled by applying Courant–Friedrichs–Lewy (CFL) condition [30]. In the present model, the droplet temperature is described through a uniform droplet model [17] for water with its high volatility. The stochastic parcel method is adopted, where the parcel mass m_k is calculated using the relation

$$m_k = \frac{4}{3}\pi\rho_l r_k^3 N_{p,k}, \tag{14}$$

where $N_{p,k}$ is the total number of droplets in the k^{th} parcel.

The Lagrangian droplet equations are coupled to the gas phase through Eq. (12), and the spray source terms are described using the PSIC model [15, 17]. The system of gas and liquid phase equations is solved through a hybrid technique [17] with appropriate boundary and initial conditions. A non equidistant rectangular numerical grid is used, which is finer in the region near the nozzle exit with a total of 78×101 grid nodes.

The next section presents the numerical results from both models with experimental data for a water spray in nitrogen.

Results and Discussion

Experimental data from TU Graz for a liquid flow rate of 80 kg/h at a cross section of 0.08 m downstream the nozzle exit are taken to start the computations, where the measurements are available at 45 radial positions separated by 1.5 10^{-3} m distance. The experimental data are classified into 100 size groups at each radial position. The data contain droplet number frequency, droplet radius, axial and radial components of droplet velocity as well as the time period during which the measurements were recorded at each radial location. These data are used to calculate the moment sets, which in turn are used to calculate the weights (number densities), radii and velocities using a product–difference algorithm [31] in order to start the computations for DQMOM. The experimental data are also used to generate a system of parcels having the properties $(\mathbf{x}_k, r_k, \mathbf{v}_k, m_k)$ for DDM. Droplet properties including size and velocity are computed using both models and compared with the experimental results at the cross sections of 0.12 m and 0.16 m away from nozzle exit. The DQMOM simulations are carried out on a PC having two Intel dual core 2.2 GHz processors with 8 GB RAM. The DDM is simulated on a PC having an AMD quad Opteron 1.8 GHz processor with 64 GB RAM. The latter PC had several jobs running simultaneously, so that the available RAM on both PCs is about identical. All simulations are run on a single processor. The computations for DQMOM and DDM take about one hour and three days, respectively.

Figures 1 and 2 show the computed and experimental profiles of the Sauter mean diameter at cross sections 0.12 m and 0.16 m away from nozzle exit. The DDM simulation result matches quite well the experiment at the center of the spray at 0.12 m away from nozzle exit, but slightly under-predicts towards the periphery of the spray.

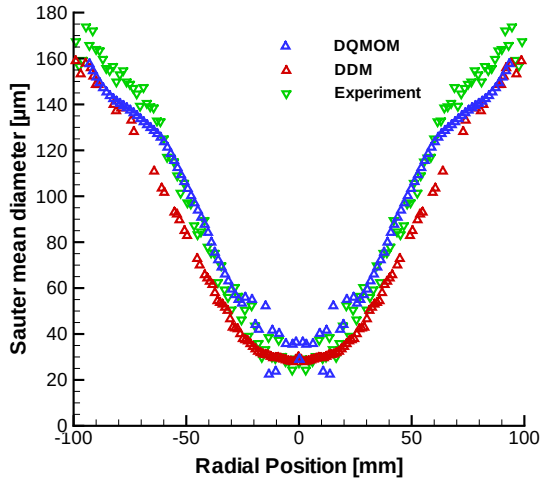

Figure 1. Experimental and numerical profiles of the Sauter mean diameter at the cross section of 0.12 m distance from the nozzle exit

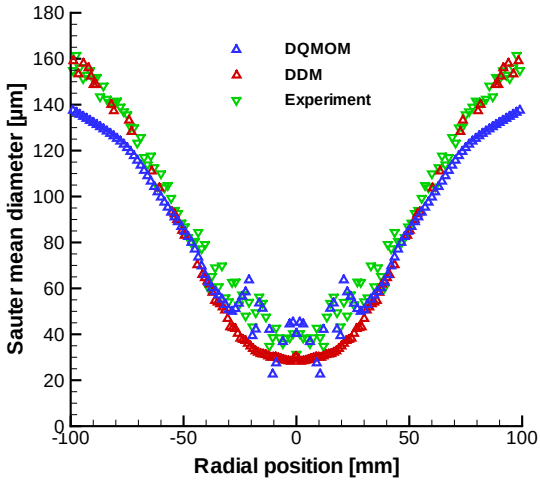

Figure 2. Experimental and numerical profiles of the Sauter mean diameter at the cross section of 0.16 m distance from the nozzle exit

A good agreement is observed at 0.16 m cross section between DDM and experiment. The DQMOM simulation results are in good agreement with experiment at 0.12 m downstream the nozzle exit, and it is closer to the experimental data at higher radial distance. Further downstream, at 0.16 m from the nozzle exit, the DQMOM simulations reveal some scattering near the centerline, and at higher radial distances, they under-predict the experimental results. This discrepancy may result from the numerical scheme which employs an explicit finite difference method to solve Eqs. (3) – (5); the results may be improved by implementing an implicit method.

The overall shape of a hollow cone spray is captured quite nicely by both methods, although some deviations are observed in particular in DQMOM as compared to experimental profile, possibly due to the post-processing of the experimental data in order to correct the number frequency at every measuring position to rule out the fluctuations in the effective cross section area of the measuring volume for the larger droplet sizes [32]. This correction of experimental data is position dependent, whereas the DQMOM and DDM results account for these

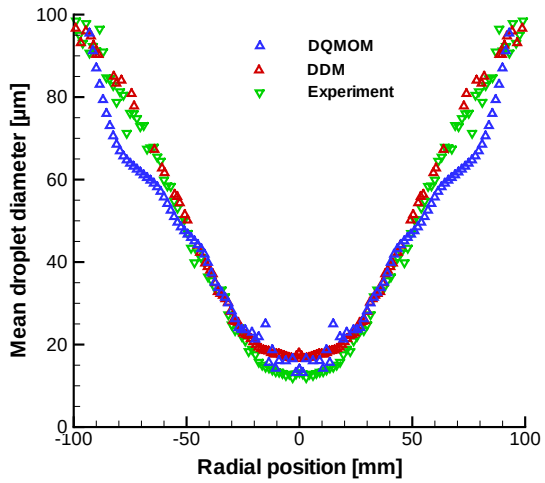

Figure 3. Experimental and numerical profiles of the mean droplet diameter at the cross section of 0.12 m distance from the nozzle exit

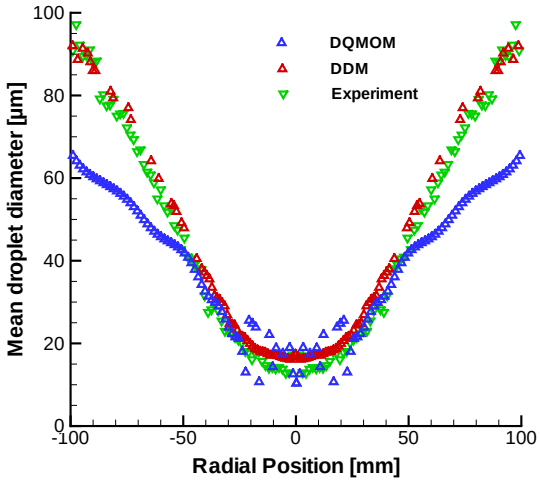

Figure 4. Experimental and numerical profiles of the mean droplet diameter at the cross section of 0.16 m distance from the nozzle exit

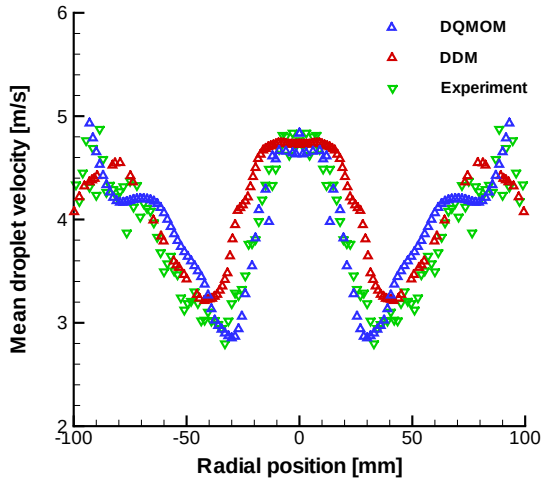

Figure 5. Experimental and numerical profiles of the mean droplet velocity at the cross section of 0.12 m distance from the nozzle exit

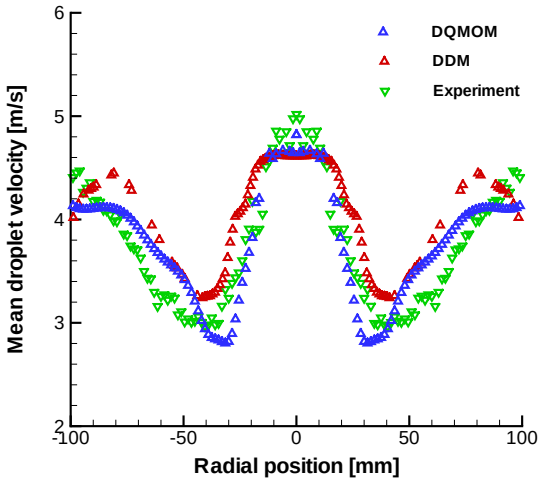

Figure 6. Experimental and numerical profiles of the mean droplet velocity at the cross section of 0.16 m distance from the nozzle exit

corrections for the initial condition but not at positions further downstream. Another reason for the discrepancies in the DQMOM results may be the fact that the spray equations are not yet fully coupled to the gas phase.

Comparing the maximum values of the Sauter mean diameter at the two cross sections displayed in Figs. 1 and 2, a decrease in large size droplets is observed as the droplets move away from nozzle. Even though the process of evaporation is considered in the present models, the major reason for the decrease in droplet size may be attributed to the influence of drag force applied by the surrounding gas, because significant evaporation may not occur at the present room temperature condition. This decrease is more evident in the large droplet size region, where the dynamic interaction of droplet with surrounding gas dominates as observed in profiles of mean droplet velocity (see Figs. 5 and 6).

Besides the Sauter mean radius, in many technical applications such as particle size analysis in powder sampling or pharmaceutical industries, the mean droplet diameter is an important physical quantity. Radial profiles of the mean droplet diameter are shown and compared with experiment in Figs. 3 and 4. DDM results coincide well with the experiment. A slight decrease in the mean droplet diameter is observed as the droplets move away from nozzle indicating some mass transfer from liquid to gas, which is attributable to gas – liquid interactions. The DQMOM results are in very good agreement with experiment at the cross section of 0.12 m near the centerline, and there, they improve the DDM results. At 75 mm radial position, the DQMOM results are below experimental values, which may stem from the explicit finite difference technique. At the cross section of 0.16 m, a good agreement is observed between DQMOM and experiment near the axis of symmetry, even though some scattering is obtained. Deviations from experiment occur in the large droplet size region, which is due to the fact that the numerical technique captures the distribution function globally, and some local discrepancies may be observed. This may be improved by solving the gas phase equations for DQMOM, which is not done in the present study, where the inlet gas flow properties are used to calculate the source terms for Eqs. (3) – (5).

In Figs. 5 and 6, the radial profiles of mean droplet velocity are displayed. It can be seen that the droplet velocity is higher for larger droplets as anticipated. Interestingly, the small size droplets near to the axis of symmetry also move at a higher velocity as observed in the experiment and thus making the velocity profile bimodal, which is predicted quite nicely by both models. A closer look reveals that the width of the jet is captured by the DQMOM, whereas the DDM predicts somewhat broader profiles with a lower maximum value at the centerline. At the spray edge, a judgement of the numerical methods is difficult, since the experimental data are somewhat spread in the case of the smaller distance from the nozzle exit. At 0.16 m, the slopes of the numerical results deviate from the experimental data, which show the highest error in experimental data processing [32]. Comparing the velocity profiles at the two different cross sections, it is seen that the velocity decreases as droplets move away from nozzle. This is because the droplets are strongly decelerated by the dynamic interaction with the surrounding gas. The gas around the spray stagnates and is driven into motion only due to the spray entrainment. The gas motion driven by the spray arises at the expense that the droplet loses momentum.

The droplet properties are predicted quite well by the present simulations, which confirms their applicability for spray flows. There are some minor deviations between simulation and experimental results. For DQMOM, the simultaneous solution of the gas phase equations may improve the simulation results.

Summary and Conclusions

In this paper, DQMOM is developed to model a dilute water spray in nitrogen, and the results are compared with a DDM and experimental data. In DQMOM, the mathematical formulation is derived, and a numerical solution procedure is developed. For DDM, the gas phase is described by Favre-averaged Navier-Stokes equations considering the droplet properties as point sources, which are calculated using the PSIC model. The effect of drag force, gravity, and evaporation on the droplet size and velocity distribution is analyzed with both methods.

Numerical results are compared with experimental results at different cross sections, where the experimental data of the cross section closest to the nozzle exit are used for the generation of initial conditions for the simulations. The results from both methods are found in good agreement with experiment. Some deviations between DQMOM and experiment in case of mean droplet diameter are observed that might have resulted from the present DQMOM formulation, which is not yet fully coupled with the gas phase equations. Moreover, the numerical technique employed an explicit finite difference method to solve the DQMOM transport equations – an implicit scheme may lead to considerable improvement. Concerning the experimental data, a post-processing of the raw data was performed in order to correct the number frequency of large droplets with respect to the effective cross section area, leading to different correction factors for different droplet positions in experimental data away from the centerline – these different corrections cannot be reflected in the numerical results.

Acknowledgements

The authors gratefully acknowledge the financial support from Deutsche Forschungsgemeinschaft (DFG) under program SPP 1423 and Heidelberg Graduate School for Mathematics and Computational Sciences at IWR. They thank Prof. G. Brenn and E. Wimmer from TU Graz, Austria for providing the experimental data and for many discussions on experimental data processing. Moreover, the help of N. Wenzel with generation of initial data for the numerical simulations is acknowledged.

References

[1] Laurent, F., Massot, M., *Combustion Theory and Modelling* 5(4): 537-572 (2001).
[2] Marchisio, D. L., Pikturna, J. T., Fox, R. O., Vigil, R. D., and Barresi, A. A., *AIChE Journal* 49: 1266-1276 (2003).
[3] McGraw, R., *Aerosol Science and Technology* 27(2): 255-265 (1997).
[4] Laurent, F., Massot, M., and Villidieu, P., *Journal of Computational Physics* 194(2): 505-543 (2004).
[5] Dufour, G., Villidieu, P., *Mathematical Modeling and Numerical Analysis* 39(5): 931-936 (2005).
[6] Marchisio, D. L., Vigil, R. D., and Fox, R. O., *Journal of Colloid and Interface Science* 258(2): 322-334 (2003).
[7] Marchisio, D. L., Fox, R. O., *Journal of Aerosol Science* 36: 43-73 (2005).
[8] Dukowicz, J. K., *Journal of Computational Physics* 2: 111-566 (1980)
[9] Bird, G. A., *Molecular Gas Dynamics and Direct Simulation of Gas Flows* Oxford Science Publications 42, 1994.
[10] Ge, H.-W., Gutheil, E., *Progress in Computational Fluid Dynamics* 7(8): 467-472 (2007).
[11] Gopireddy, S. R., Humza, R. M., and Gutheil, E., *Chemie Ingenieur Technik* 84(3): 349-356 (2012).
[12] Law, C. K., *Progress in Energy and Combustion Science* 8: 171-201 (1982).
[13] Abramzon, B., Sirignano, W. A., *International Journal of Heat and Mass Transfer* 32(9): 1605-1618 (1989).
[14] Tratnig, A., Brenn, G., *International Journal of Multiphase Flow* 36(5): 349-363 (2010).
[15] Crowe, C. T., Sharma, M. P., and Stock, D. E., *Journal of Fluids Engineering* 99: 325-332 (1977).
[16] Williams, F. A., *Physics of Fluids* 1: 541-545 (1958).
[17] Hollmann, C., Gutheil, E., *Proceedings of Combustion Institute* 26(1): 1731-1738 (1996).
[18] Fox, R. O., Laurent F., and Massot, M., *Journal of Computational Physics* 227(6): 3058-3088 (2008).
[19] Chan, T. L., Liu, Y. H., and Chan, C. K., *Journal of Aerosol Science* 41: 553-568 (2010).
[20] Selma, B., Bannari, R., and Proulx, P., *Chemical Engineering Science* 65(6): 1925-1941 (2010).
[21] Mezzei, L., Marchisio, L., and Lettieri, P., *Industrial Engineering and Chemistry Research* 49(11): 5141-5152 (2010).
[22] Bruyat, A., Laurent, C., and Rouzand, O., *International Conference on Multiphase Flow*, Tampa, Florida, May 30 - June 4, 2010.

[23] Choi, D., Schneider, L., Spyrou, N., Sadiki, A., and Janicka, J., *International Conference on Multiphase Flow*, Tampa, Florida, May 30 - June 4, 2010.
[24] Atkins, P., Paula, J. D., *Atkins' Physical Chemistry* Oxford Higher Education, 7$^{\mathrm{th}}$ Edition, 2001.
[25] Antoine, C., *Comptes Rendus des Séances de l'Académie des Sciences* 107: 681-684 (1888).
[26] Batchelor, G. K., *An Introduction to Fluid Dynamics* Cambridge University Press London, 1967.
[27] Schiller, L., Neumann, A. Z., *VDI Zeitschrift* 77: 318-320 (1933).
[28] Sirignano, W. A., *Journal of Fluids Engineering* 115: 345-378 (1992).
[29] Faeth, G. M., *Progress in Energy and Combustion Science* 9: 1-76 (1983).
[30] Courant, R., Friedrichs, K., Lewy, H., *Mathematische Annalen* 100(1): 32-74 (1928).
[31] Gordon, R. G., *Journal of Mathematical Physics* 9: 655-663 (1968).
[32] Albrecht, H.-E., Damaschke, N., and Tropea, C., *Laser Doppler and Phase Doppler Measurement Techniques* Springer-Verlag, Berlin, 2003.